NRC Research Press

ARTICLE

Improved understanding of geogrid response to pullout loading: insights from three-dimensional finite-element analysis

Mahmoud G. Hussein and Mohamed A. Meguid

Abstract: Soil reinforcement has rapidly become one of the most common soil improvement techniques used in geotechnical engineering. Understanding the behavior of a geogrid under pullout loading is essential for the analysis and design of reinforced soil systems. The overall behavior of reinforced soils is generally dependent on the properties of the geogrid material, the backfill soil, and the interface condition. Modeling the three-dimensional aspects of soil–geogrid interaction under pullout loading condition is numerically challenging and requires special consideration of the different modes of resistance that contribute to the pullout capacity of the geogrid reinforcement. This study describes the results of a three-dimensional finite-element analysis that has been developed to investigate the behavior of a biaxial geogrid embedded in granular backfill material and subjected to pullout loading. The modeling approach considers the noncontinuous nature of the geogrid geometry and the elastoplastic response of the geogrid material. Model validation is performed by simulating laboratory-size pullout test and comparing the experimental data with the analytical as well as numerically calculated results. The detailed behavior of the geogrid and the surrounding backfill is investigated using the proposed numerical approach. Conclusions are made to highlight the suitability of this technique for analyzing similar soil–structure interaction problems.

Key words: geosynthetics, biaxial geogrid, pullout test, soil–geogrid interaction, frictional resistance, bearing resistance, nonlinear contact.

Résumé : Le renforcement des sols est rapidement devenu l'une des techniques d'amélioration des sols les plus couramment utilisées en génie géotechnique. La compréhension du comportement de la géogrille sous charge d'arrachement est essentielle pour l'analyse et la conception des systèmes de sols renforcés. Le comportement général des sols renforcés dépend généralement des propriétés du matériau de la géogrille, du sol de remblai et de l'état de l'interface. La modélisation des aspects tridimensionnels de l'interaction sol–géogrille dans des conditions de charge d'arrachement est un défi numérique et nécessite une attention particulière aux différents modes de résistance qui contribuent à la capacité d'arrachement de l'armature géogrille. Cette étude décrit les résultats d'une analyse tridimensionnelle par éléments finis qui a été mise au point pour étudier le comportement d'une géogrille biaxiale noyée dans un matériau de remblai granulaire et soumise à une charge par arrachement. L'approche de modélisation tient compte de la nature non continue de la géométrie de la géogrille et de la réponse élastoplastique du matériau de la géogrille. La validation du modèle s'effectue en simulant un essai d'arrachement de la taille d'un laboratoire et en comparant les données expérimentales avec les résultats analytiques et les résultats calculés numériquement. Le comportement détaillé de la géogrille et du remblai environnant est étudié à l'aide de l'approche numérique proposée. Des conclusions sont tirées pour souligner la pertinence de cette technique pour analyser des problèmes d'interaction sol–structure similaires. [Traduit par la Rédaction]

Mots-clés : géosynthétiques, géogrille biaxiale, test d'arrachement, interaction sol–géogrille, résistance au frottement, résistance portante, contact non linéaire.

Introduction

Geosynthetic reinforcements are used in various geotechnical engineering applications, including reinforced earth fills, retaining walls, embankments, paved roads, and foundations. The use of geosynthetics is known to improve soil performance: increasing the safety factor against shear failure while reducing the construction cost of the project (Koerner 2012). In general, evaluating soil–geosynthetic interaction response is relatively complex as it is affected by several factors including (*i*) geometrical and mechanical characteristics of the geosynthetic material, (*ii*) mechanical properties of soil, and (*iii*) boundaries and loading conditions. When using a continuous geotextile (sheet) to reinforce soils, skin friction is the only mechanism that develops at the soil–geotextile interface, while for geogrids, and due to its open structure, the interaction becomes more complex (Moraci et al. 2014). The interaction between granular soils and extensible geogrids used in reinforced geotechnical systems has been the subject of extensive research (e.g., McGown et al. 1984). Soil–geogrid interaction involves three basic load transfer mechanisms: (*i*) tangential–skin friction, which is a three-dimensional frictional resistance between the geogrid elements (longitudinal ribs and transversal bars) and the surrounding backfill; (*ii*) passive earth pressure (bearing resistance) on the transversal bars; and (*iii*) interlocking of grain particles inside the grid openings (soil-to-soil friction). Depending on the loading condition and the geosynthetic geom-

Received 10 June 2018. Accepted 3 April 2019.

M.G. Hussein and M.A. Meguid. Department of Civil Engineering and Applied Mechanics, McGill University, Montréal, Quebec, Canada.
Corresponding author: Mohamed A. Meguid (email: mohamed.meguid@mcgill.ca).

etry, one or more of these interaction mechanisms can be mobilized.

Two design criteria are generally used for most reinforced-soil structures: (*i*) the reinforcement must not fail in tension (by rupture or excessive deformation) and (*ii*) the reinforcement must not pull out of the soil-resistant zone (Lentz and Pyatt 1988). Designing against tensile failure requires that tensile stresses in the reinforcement be less than the ultimate strength of the material. To satisfy the pullout failure criterion, which is generally applied in reinforced walls and slopes, it is required to determine the reinforcement anchorage capacity and the appropriate reinforcement length and spacing to prevent pullout failure. In addition, connection failure between the reinforcement layer and the wall-facing needs to be considered in the analysis.

Soil–geogrid interaction under pullout loading

Pullout tests generally provide capacity values for specific reinforcement, soil, and load conditions. They also allow for the coefficient of interaction, which is of primary interest in design, to be determined accurately. According to AASHTO (2012), the coefficient of interaction is a mass parameter that combines the effect of all interaction mechanisms.

Several limit equilibrium–based models to estimate geogrid pullout capacity have been developed by researchers (e.g., Jewell et al. 1984; Koerner et al. 1989; Palmeira and Milligan 1989; Gurung and Iwao 1999; Perkins and Cuelho 1999; Moraci and Gioffrè 2006; Weerasekara et al. 2017; Zornberg et al. 2017). Most of these models calculate the pullout capacity of a geogrid as the cumulative contribution of the mobilized bearing resistances at the transversal bars and frictional resistances along the surface area of the geogrid (friction along the longitudinal and transversal elements). The pullout resistance is generally expressed as follows:

$$P = P_{s/r} + P_{pb} \quad (1)$$

where P is the pullout resistance, $P_{s/r}$ is the frictional resistance between the soil and the in-plane surface area of the reinforcement, and P_{pb} is the passive bearing resistance of the bearing members. In addition to limit equilibrium models, pullout capacity models commonly used in North America are based on both the AASHTO (2012) and the FHWA (Berg et al. 2009) design specifications. The procedure lumps the contributions of both frictional and bearing resistance into a single nondimensional parameter called the "pullout resistance factor", F^*, also called the "coefficient of interaction parameter" according to FHWA (Berg et al. 2009). In this method, the pullout capacity is estimated as

$$P = 2L_e\sigma_v F^*\alpha \quad (2)$$

where P is the pullout resistance per unit width of the geogrid, L_e is the length of reinforcement in the resisting zone (anchorage length), σ_v is the normal stress at the reinforcement level, F^* is the pullout resistance factor (coefficient of interaction = $\frac{2}{3}\tan\phi$), and α is a scale effect correction factor (0.8 for geogrids and 0.6 for geotextiles).

Soil–geogrid interface

The shear stress–strain relationship along a given soil–geogrid interface, which is used to determine the required anchorage length, is commonly characterized using direct shear and (or) pullout tests (Farrag et al. 1993). Direct shear tests are applicable for conditions involving a failure plane that propagates mainly along the reinforcement (direct sliding mechanism) and are used to determine the frictional bond between the backfill soil and the surface area of the geogrid (Fig. 1). Pullout tests, in contrast, are used to study the anchorage capacity of a geogrid reinforcement

Fig. 1. Pullout and direct sliding mechanisms. [Color online.]

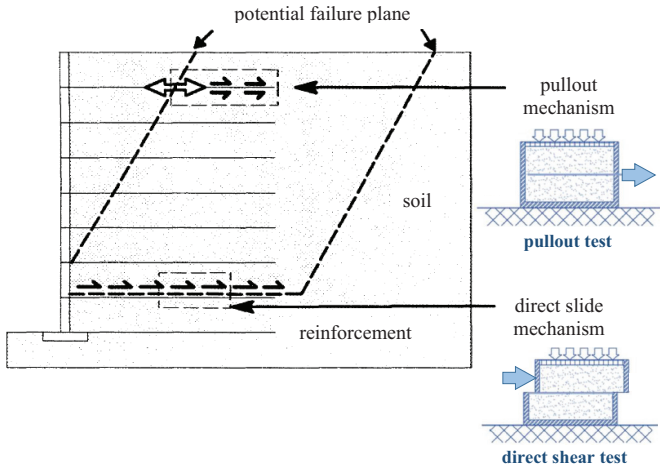

and to understand the load-transfer mechanism within the anchorage zone.

Another distinction between the two tests relates to how strains mobilize along the surface of the reinforcement. For direct shear tests, the mobilized shear strains are postulated to be distributed uniformly along the soil–geogrid interface; while in pullout tests, the mobilized strains are combination of interface shear strains and geogrid extension. This coupled mechanism results in a nonuniform shear strain–stress distribution along the geogrid.

Modeling pullout tests

In North America, ASTM (2013) standard D6706-01 is used to quantify pullout capacity in the laboratory. A large amount of literature related to the results and interpretation of pullout laboratory tests is available (Palmeira and Milligan 1989; Farrag et al. 1993; Bakeer et al. 1998; Alagiyawanna et al. 2001; Moraci and Recalcati 2006; Lopes and Silvano 2010; Hatami et al. 2013; Ferreira et al. 2015; Bathurst and Ezzein 2016; Cardile et al. 2016; Abdi and Mirzaeifar 2017; Kayadelen et al. 2018). The effects of several factors, such as the pullout box size, front and sidewall conditions, sleeve length, soil and reinforcement properties, test speed, and applied normal stress on the pullout test results, have been evaluated. In most of these investigations, the focus has been on understanding the mechanisms of soil–structure interaction, development of pullout models of varying complexity, and refining the test methodology to ensure consistent and reliable estimates of the pullout capacity. However, the number of reported tests has been limited and often restricted to one type of geosynthetic product or one product line.

Several attempts have been made to develop analytical models to estimate soil–geosynthetic interaction under pullout loading conditions (e.g., Jewell et al. 1984; Koerner et al. 1989; Palmeira and Milligan 1989; Gurung and Iwao 1999; Perkins and Cuelho 1999; Moraci and Gioffrè 2006; Berg et al. 2009; Cardile et al. 2017). The theoretical expressions used in these models to evaluate the pullout resistance and the associated soil–geogrid interaction coefficient show some limitations. In particular, these models do not take into account the true reinforcement geometry and extensibility and the soil dilatancy that strongly affect the pullout behavior.

While it is possible to track the load–displacement response of a geogrid layer in pullout experiments, the behavior of the backfill soil as it interacts with the geogrid material is difficult to evaluate experimentally (Meguid 2014). Numerical methods are, therefore, considered more suitable for that purpose. The discrete element (DE) method has been used by several researchers to model soil–geogrid interaction (McDowell et al. 2006; Zhang et al.

2008; Bhandari and Han 2010; Chen et al. 2012; Wang et al. 2016; Miao et al. 2017; Xu and Liang 2018). In this approach, the geogrid is simulated using a set of spherical particles bonded together to form the geogrid shape. The interaction between the geogrid and the surrounding soil is obtained through the contact between discrete particles. Although microscopic parameters of the bonded geogrid particles are determined using index tests, the complex geogrid deformation may not be calculated accurately due to the inflexibility of the discrete particles. Moreover, as bonded particles are used to model the continuous nature of the geogrid, the strains and stresses developing in the geogrid may not be obtained accurately.

Tran et al. (2013) introduced an approach to simulate the pullout test by coupling both the finite (FE) and DE methods. In this procedure, the reinforcement layer is modeled using finite elements whereas the backfill soil is modeled using discrete elements. The coupling of the two methods can efficiently model the behavior of both the geogrid and backfill material. Although the coupled model was able to capture the important features of the problem, the method was limited in considering the geogrid as a linear elastic material.

The FE method has been used extensively to analyze soil–structure interaction associated with the pullout procedure (e.g., Yuan and Chua 1990; Wilson-Fahmy and Koerner 1993; Shuwang et al. 1998; Perkins and Edens 2003; Sugimoto and Alagiyawanna 2003; Siriwardane et al. 2008; Chen et al. 2011; Abdi and Zandieh 2014; Hegde and Roy 2017; Gu et al. 2018; Touahmia et al. 2018). In these studies, the geogrid geometry is often simplified either as a truss structure (in two-dimensional analysis) or as a continuous sheet (in three-dimensional (3D) analysis). These simplifications make it difficult to separate the contributions of the frictional and bearing resistances with respect to the overall pullout capacity of a geogrid-reinforced system.

In an attempt to capture the detailed geometry of an embedded geogrid, Hussein and Meguid (2009, 2013) modelled the geogrid pullout test using 3D FE analysis. The geogrid was simulated using a nonlinear elastoplastic constitutive model that separates the elastic and plastic strains. The analysis was performed using six-noded solid elements for the soil and three-noded triangular membrane elements for the geogrid. The details of the grid apertures were taken into account when capturing the discontinuous nature of the geogrid. Although the FE analysis, conducted using explicit 3D geogrid geometry, has reasonably captured the pullout response and predicted a load–displacement relationship that is consistent with the experimental data, the model response was only reliable at the front face of the box as stresses and displacements inside the model were not consistent with the measured results.

The objective of this study is to introduce a FE approach that is suitable for analyzing soil–geogrid interaction under pullout loading conditions. This numerical framework aims at simulating the detailed geometry and material properties of both the geogrid and the surrounding backfill in three dimensions. The model is capable of capturing the severe nonlinearity of the system caused by the contact and the large relative movements at the soil–geogrid interface. Although emphasis is placed in this study on evaluating the contributions of the frictional and bearing components of the pullout resistance, displacements, stresses, and strain fields near the geogrid are also evaluated. The results of the numerical analysis including the detailed response of the geogrid and the surrounding soil are compared with experimental data. The 3D FE analyses presented in this study have been performed using the general FE software ABAQUS/Standard, version 6.13 (Dassault Systems Simulia Corp. 2013).

Numerical analysis

The numerical approach presented in this study is an extension of the one reported by Hussein and Meguid (2016). A case study involving pullout experiments performed on a biaxial geogrid (Sugimoto and Alagiyawanna 2003) is carefully selected and used throughout this investigation.

Description of pullout tests

The test setup involved a soil container measuring 0.52 m in length, 0.3 m in width, and 0.625 m in height. The front wall comprised six acrylic plates 0.3 m × 0.1 m to reduce the soil–wall friction. The soil used in the experiment was silica sand No. 5 with average particle diameter D_{50} = 0.34 mm and a peak friction angle of 29.9° (relative density, D_r = 70%) that was determined using laboratory triaxial tests. A biaxial geogrid sample 500 mm in length and 300 mm in width was used in the experiments (with material and geometry similar to that presented by Hussein and Meguid (2016)). The sand was placed in layers using the raining technique and the pullout load was applied through a clamp attached to the front side of the geogrid sheet. Vertical stresses of 49 and 93 kPa were applied above and below the box, respectively, using air bags to prevent vertical movement of the geogrid during the test. The geogrid was pulled out at a constant rate of 1.0 mm/min and both the load and lateral movement were measured using load cells and displacement gauges, respectively.

Model generation

The numerical model has been developed such that it follows the geometry and test procedure used in the experiment. Details related to the different aspects of the model are given below.

Geogrid model

The exact geogrid geometry (eight longitudinal ribs and 19 transverse bars) was modeled using eight-noded linear brick elements with eight integration points (Fig. 2). The elastoplastic material model developed by Hussein and Meguid (2016) for the biaxial geogrid is used throughout this analysis. The geogrid properties are summarized in Table 1. A nondeformable clamp is introduced at the front side of the geogrid. The clamp is treated as linear elastic material with density of 7850 kg/m^3, Poisson's ratio of 0.3, and Young's modulus of 200 GPa. The geogrid is simulated using over 6430 finite elements as shown in Fig. 2. It should be noted that the local increase in joint thickness is not considered in the geogrid model to simplify the nonlinear contact analysis. This approximation is expected to cause a slight reduction in bearing resistance that would develop at these particular locations.

Backfill model

The sand used in the experiment was modeled using elastoplastic Mohr–Coulomb (MC) failure criteria with a nonassociated flow rule and the soil domain was discretized using eight-noded linear brick elements (C3D8). The input parameters used in the FE analysis are summarized in Table 2. Soil dilation is integrated into the model using the classical stress–dilatancy framework proposed by Bolton (1986).

The extended Mohr–Coulomb (EMC) model available in ABAQUS is an extension of the classical MC failure criterion. It is an elastoplastic model that uses the yield function of the MC form in addition to a hardening law and a flow rule. The yield function includes isotropic cohesion hardening–softening. However, the model uses a flow potential that has a hyperbolic shape in the meridional stress plane and a piecewise elliptic shape (with no corners) in the deviatoric stress space. This flow potential, which is continuous and smooth in the deviatoric and meridional stress planes, ensures that the flow direction is always uniquely defined in this plane.

Although soil material generally behaves nonlinearly with stress-dependant stiffness and the ABAQUS MC model may not

Fig. 2. Plan view of geogrid mesh and geometry for pullout model. [Color online.]

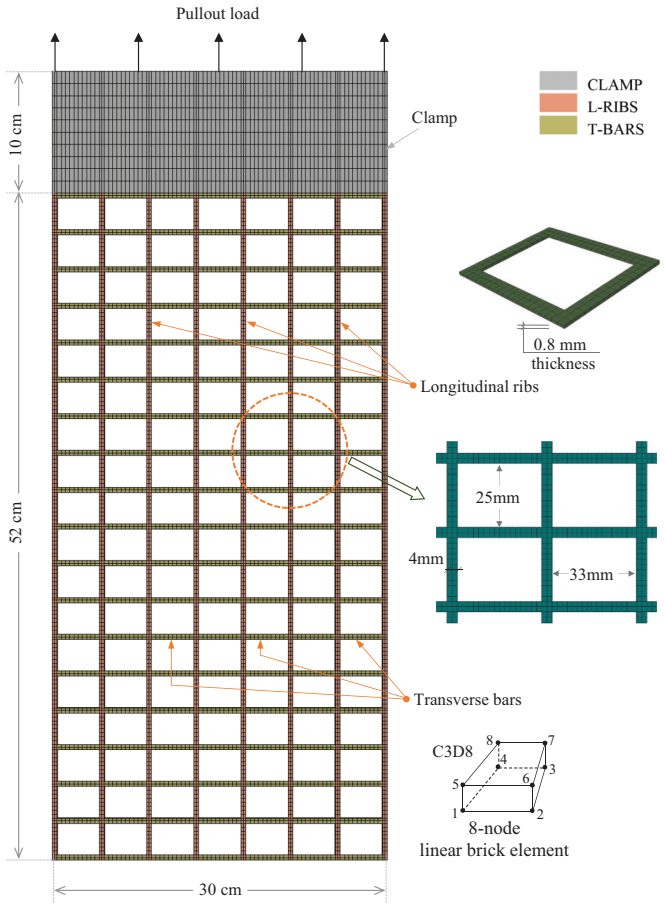

consider the variation of elastic modulus with stress, the model is considered to be acceptable for the current application. It should be noted that, during the pullout process, particle interlocking can cause a significant increase in normal stresses at the soil–reinforcement interface. This behavior may not be captured accurately by the adopted model.

Modeling procedure

The model was divided into four main domains as shown in Fig. 3. The bottom soil domain (BS) was first generated in three stages (around 10 cm each) and the geostatic stress state was established for each stage. Then, the geogrid (GEO) was added and the soil elements needed to fill the openings ($Soil_{OPN}$, with a thickness of 0.8 mm) were introduced in a separate step. Finally, the top soil domain (TS) of around 30 cm in thickness was generated in stages (around 10 cm each) to reach the soil surface. A partial view of the 3D mesh is presented in Fig. 3 with half of the top soil removed for illustration purposes. It is worth noting that soil elements located above and below the geogrid can interact directly with each other through the soil elements present in the openings ($Soil_{OPN}$) leading to soil continuity, which closely models the geogrid embedment in the backfill material. This is achieved numerically by merging the three soil domains together, using the meshing *merge* tool in ABAQUS, to form one soil part.

Sensitivity analysis was first conducted using different element sizes to determine a suitable mesh refinement that brings a balance between accuracy and computing time. The 3D FE mesh, with over 153 170 elements, is shown in Fig. 3. The mesh size was adjusted in the vertical direction around the geogrid to provide sufficient resolution in the interaction area. Boundary conditions were defined such that nodes along the vertical boundaries may only translate freely in the vertical direction (smooth rigid). Nodes at the base are fixed against displacements in all directions (rough rigid). Details related to the development of the FE model can be found elsewhere (Hussein 2016).

Contact analysis

Modeling soil–geogrid interaction is considered to be one of the challenging tasks in this analysis. The pullout experiment generally involves large deformations that lead to relative movements between the geogrid and the surrounding backfill. This results in a severe nonlinear response at the contact in addition to other sources of material nonlinearity due to the adopted geogrid and soil models. Moreover, modeling the contact interface in three dimensions requires careful attention to the details so that the analysis can be completed successfully within a reasonable time. Figure 4 shows the modeling approach used to simulate the soil–geogrid interaction in this study. This contact interaction is enforced through the master-slave contact pair technique available in ABAQUS. Additional model details are given below.

Master-slave contact pair

The master-slave contact pair approach is a surface-based contact simulation in which surfaces for the bodies that could potentially be in contact during the analysis are first defined. Then, the mechanical contact property models that will control the relationship between the contacting bodies are assigned. In doing so, one surface in the contact pair is designated to be the slave surface and the other is the master surface. It is suggested that the body with the finer mesh be treated as the slave while the body with coarser mesh be the master. In the current study, the soil domain above (and below) the geogrid and inside the apertures was coarser and therefore, the soil was taken as the master surface and the geogrid as the slave surface.

Contact interaction

To define the contact between any pair of surfaces, three main aspects need to be addressed. First, how the contact constraints are defined (discretized); then, how the constraints are enforced; and finally, how the constraints evolve upon sliding.

Contact discretization

ABAQUS offers two types of contact discretization; namely, (*i*) surface-to-surface and (*ii*) node-to-surface. In the surface-to-surface formulation, the contact condition is enforced in an average sense over regions in the vicinity of the slave nodes rather than only at individual nodes. In contrast, in the node-to-surface discretization method, each contact condition involves a single slave node and a group of nearby master nodes (master facet).

In the current study, surface-to-surface contact discretization was chosen to simulate soil–geogrid interaction. Enforcing the contact in an average sense over a region surrounding each slave node was found to produce more accurate contact stresses, and results in a better convergence of the analysis.

Constraints enforcement

When surfaces are in contact, they usually transmit shear (tangential) as well as normal forces across the interface. There is generally a relationship between these two force components. In a mechanical contact simulation, the interaction between contacting bodies is usually defined by assigning a contact property model to the concerned interaction. In this study, two types of constitutive models are used; namely, (*i*) friction model and (*ii*) contact pressure–overclosure (penetration and (or) clearance). The friction model is used to induce frictional stresses that resist sliding, while the contact pressure–overclosure model controls the contact pressure that resists penetration in the normal direction. Both models are used simultaneously for any contact pair

Table 1. Properties of biaxial geogrid.

Aperture size (mm)		Specimen size (mm)		No. of members		Ultimate strength (kN/m)		Stiffness at 2% strain (kN/m)		
Long.	Trans.	Length	Width	Long.	Trans.	Long.	Trans.	Long.	Trans.	Mass/unit area (g/m²)
29	37	500	300	8	19	12	20	204	292	215

Note: Long., longitudinal; Trans., transverse.

Table 2. Soil input parameters used in FE analysis of pullout test.

Elastic modulus, E (MPa)	Poisson's ratio, ν	Peak friction angle, ϕ_p (°)	Critical state friction angle, ϕ_{cv} (°)	Dilatancy angle, ψ (°)[a]	Cohesion (MPa)
50	0.3	29.9	28	3	1×10⁻⁵

[a]Determined using Bolton's (1986) equation.

Fig. 3. Details of 3D mesh geometry for pullout modeling. CLAMP, rigid loading clamp. [Color online.]

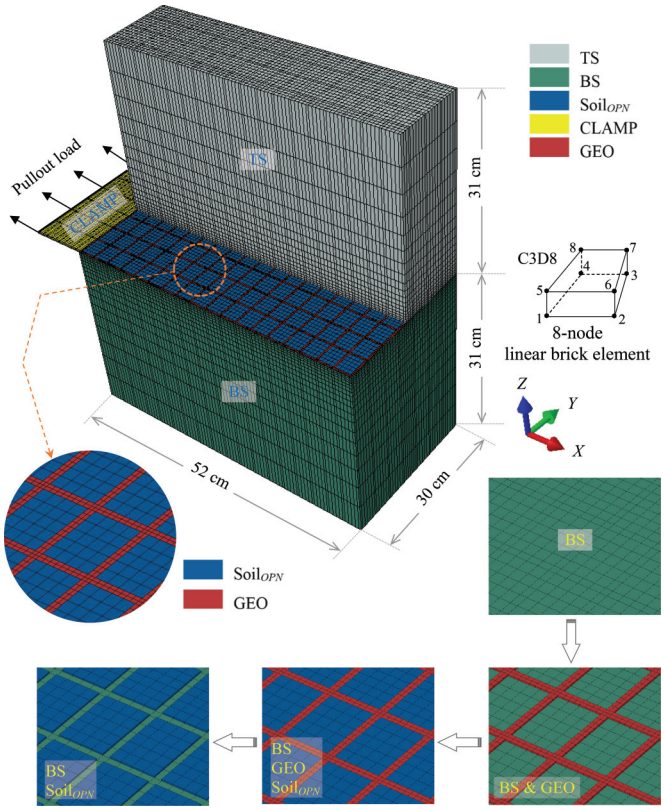

involved in the analysis. A detailed description of these constitutive models is given below.

Friction model

The friction model defines the force that resists the relative tangential motions of the contacting surfaces. In ABAQUS, there are several options available to describe the stick–slip discontinuity (frictional behavior) condition in the tangential direction. Among these options is the Coulomb friction model with normal stress-dependent friction coefficient. This model has been used in the current study to simulate the frictional resistance between the soil and the geogrid.

Coulomb friction model — The basic concept of the Coulomb friction model is that every two contacting surfaces can carry shear stresses up to a certain magnitude ($\tau_{critical}$) across their interface before they start sliding relative to one another; this state is

Fig. 4. Details of soil–geogrid interaction (after Hussein and Meguid 2016). [Color online.]

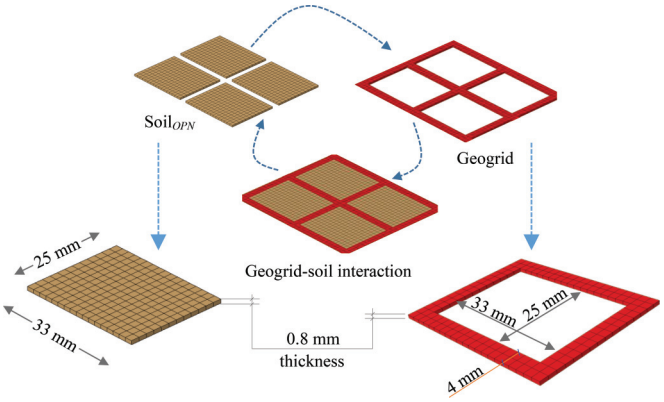

known as sticking (Fig. 5*a*). The model obeys the Mohr–Coulomb failure criterion such that

$$\tau_{critical} = c + \sigma_n \tan\delta \quad (3)$$

where $\tau_{critical}$ is the shear strength at which the slip occurs for the first time, c is the apparent cohesion, σ_n is the normal stress, and δ is the interface friction angle at the yield–critical state.

The interface friction angle (δ) between the sand and the geogrid can be obtained using direct shear tests as shown in Fig. 5*b*. Hence, the frictional interface coefficient ($f_{ds} = \tan\delta/\tan\phi$) can be calculated knowing the values of δ and the sand friction angle (ϕ). Subsequently, the value of the coefficient of friction can be determined ($\mu_{sand/geogrid} = \tan\delta$).

In the ABAQUS Coulomb friction model, the sticking constraints at a given interface (Fig. 5*a*) can be enforced using the Lagrange multiplier contact algorithm. In this method, no relative motion develops between the two closed surfaces until the shear stress $\tau = \tau_{critical}$. However, Lagrange multipliers increase the computational cost of the analysis by adding more degrees of freedom to the model and often by increasing the number of iterations required to obtain a converged solution. In contrast, the penalty function method (stiffness method) is also available in the Coulomb friction model and is used in the present study. As shown in Fig. 5*c*, the penalty contact algorithm introduces a softer constraint through a penalty parameter (tangential or shear stiffness, k_s) that relates the frictional forces to slip displacement. The method allows some relative motion of the surfaces (an elastic slip) when they should be sticking. While the surfaces are sticking (i.e., $\tau < \tau_{critical}$), the magnitude of sliding is limited to this elastic slip (E_{slip}). Within this elastic stick condition, if the tangential load is removed, the body returns to its original state. The advantage of using the penalty function method is that it is easy to implement and does not require solving nonlinear systems of equations in every time step.

The Coulomb friction model used in this study, in its simplest form, contains two material properties: a friction coefficient (μ) and a tolerance parameter to calculate the elastic slip (E_{slip}). Previous research recommends values of 0.9–1.0 for the frictional

Fig. 5. Description of the Coulomb friction models used in this study. [Color online.]

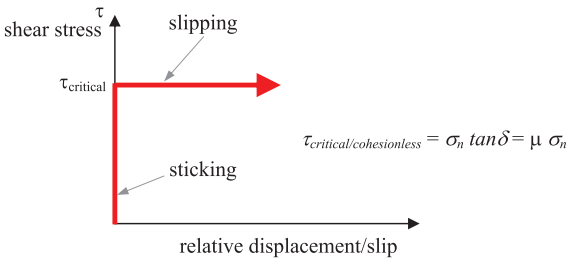

a) Coulomb friction model in its basic form

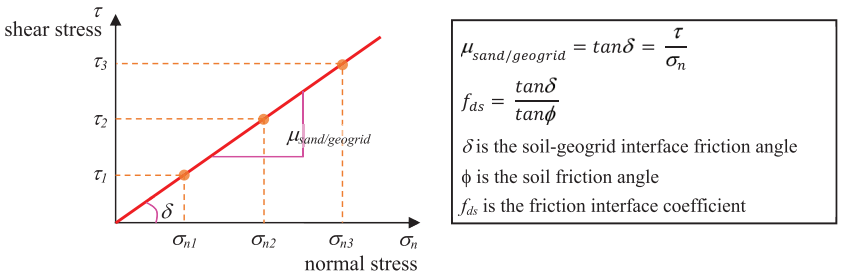

b) Parameters of direct shear test on soil-geogrid interface

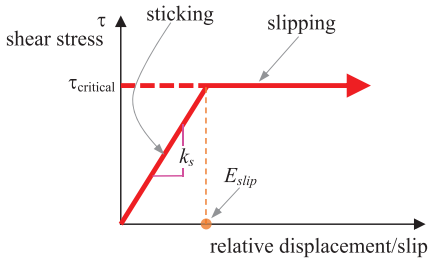

c) Coulomb friction model using the penalty contact algorithm

interface coefficient (f_{ds}) between the geogrid and sandy soils (Lopes et al. 2001; Liu et al. 2009). In the present analysis a value of 0.9 was chosen, which corresponds to a coefficient of friction (μ) equal to 0.51, knowing that the friction angle (ϕ) of the backfill is 29.9°.

Contact pressure–overclosure model

This model is used to control the contact pressure that resists penetration. Open–closed discontinuity in the normal direction is similar to the stick–slip discontinuity in the friction model. Several models are available in ABAQUS to describe the contact behavior in the normal direction (contact-pressure overclosure) of two contacting surfaces. Figure 6 illustrates the most common models used to simulate the contact pressure–overclosure relationship: the hard contact and the softened contact models.

In this study, both models were simultaneously used at several locations along the soil–geogrid interface. Constraints in the hard contact model (Fig. 6*a*) used in the analysis is enforced using the augmented Lagrange method. No contact pressure develops until nodes are in contact (gap distance, $h = 0$), and once the contact has been established between the contacting surfaces, unlimited contact pressure can be transmitted. The surfaces start to separate ($h < 0$) if the contact pressure reduces to 0 (or if the normal stress becomes tensile). The contact is re-established again when the clearance between them reduces to 0.

The linear softened contact model is also used to enforce the contact in the normal direction using the penalty stiffness method. This model describes a contact pressure–overclosure relationship in which the contact pressure is a linear function of the penetration between the surfaces. The surfaces transmit contact pressure when the overclosure–penetration, measured in the contact (normal direction), is greater than 0. As depicted in Fig. 6*b*, the slope of this contact pressure–overclosure relationship describes a constant penalty stiffness parameter (normal–contact stiffness, k_n) in the normal direction. The surfaces start to separate ($h < 0$) if the contact pressure reduces to 0 or tensile stresses started to develop. The softened contact model is preferred in cases of large penetration as it makes it possible to resolve the contact condition. In addition, the numerical softening associated with the penalty method can mitigate the overconstraint issues and reduce the number of iterations required for model convergence.

Based on the above discussion, it is evident that hard contact model is preferred at particular locations along the soil–geogrid interface where penetration is prevented in the normal direction. The linear softened contact model with a specific contact stiffness value is used when penetration is allowed in the normal direction (e.g., contact pressure developing along the transverse bars during pullout while penetration of the geogrid into the soil is allowed in the pullout direction).

Fig. 6. Contact behavior in normal direction. [Color online.]

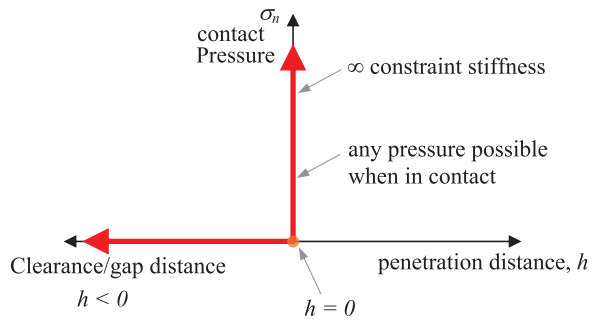

a) Hard contact model
(Constraints enforced with Lagrange multiplier method in the normal direction)

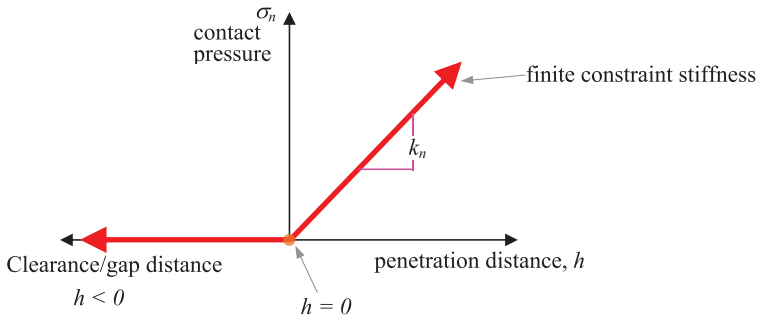

b) Linear softened contact model
(Constraints enforced with the penalty method in the normal direction)

Evolution of surface contact

There are two tracking approaches available in ABAQUS to account for the relative motion of two interacting surfaces. The first is a rigorous, nonlinear evolution (finite-sliding) while the other is an approximate formulation (small-sliding).

Small-sliding contact assumes that there will be relatively *little* sliding of one surface along the other and is based on linearized approximation. Although the approach brings less nonlinearity and is intended to reduce the solution cost and find a converged solution in fewer iterations, the method has a very limited applicability. This is due to the assumption that the relative tangential motion should remain small throughout the analysis.

Finite-sliding contact, in contrast, is the most general tracking approach and allows for arbitrary relative separation, sliding, and rotation of the contacting surfaces. It includes nonlinear geometric effects suitable for simulations that involve large deformations–rotations. As the investigated pullout problem involves large deformation, the finite-sliding tracking formulation is adopted in the analysis.

Assignment of contact models

When two bodies are in contact, normal as well as shear forces develop at the interface between the contacting bodies. The formulation used to describe the tangential and normal behavior should include separate constitutive models to simultaneously capture the two different behaviors. This means that the contact formulation detects bodies that may come into contact at any time during the course of the analysis and applies the constitutive models in the normal and tangential directions to the interface. Based on this hypothesis, the current model incorporates the two interface conditions (Fig. 7) as described below.

Horizontal soil-to-geogrid interface

This interface condition defines the contact between the horizontal geogrid surfaces — on the longitudinal ribs (HL) and transverse bars (HT) — and the horizontal surfaces of the top and bottom soils that will be in direct contact with geogrid surfaces (Fig. 7*a*). During pullout loading, the applied vertical stresses (σ_v = 49 kPa) will cause normal–contact pressure on the horizontal interfaces. At the same time, the pullout loading creates shear stresses on the same interface surfaces. The Coulomb friction model with penalty contact algorithm (Fig. 5*c*) is used to simulate the frictional behavior along the interface using a friction coeffi-

Fig. 7. Horizontal and vertical interface conditions. [Color online.]

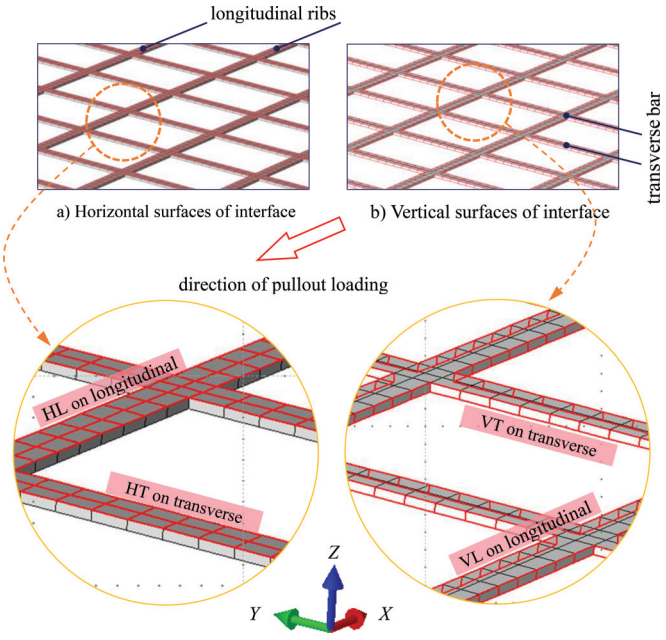

cient (μ) of 0.51. In addition, and on the same interface, a *hard* contact model (Fig. 6*a*) is imposed to simulate the contact pressure in the normal direction. The hard contact is selected to prevent penetration between the soil and the geogrid and maintain the geogrid in its vertical location during the pullout process.

The frictional resistance on this horizontal soil–geogrid interface, which is dependent on the contact pressure, is considered the frictional component of the total pullout capacity of the analyzed model.

Vertical soil-to-geogrid interface

This interface condition defines the contact between the vertical surfaces inside the geogrid apertures — on the longitudinal ribs and transverse bars — and the vertical sides of the soil elements ($Soil_{OPN}$) within the geogrid apertures (Fig. 7*b*).

As mentioned earlier, the contact formulation on each interface is simulated with frictional and normal contact constitutive models. Within the geogrid apertures, there are two vertical interface conditions (Fig. 7*b*); namely, (*i*) the vertical interface on the surfaces of the longitudinal ribs (VL) and (*ii*) the vertical interface on the surfaces of the transverse bars (VT).

Longitudinal ribs — For VL, the frictional resistance dominates the contact interaction that contributes to the pullout resistance. This friction is simulated using the Coulomb friction model similar to that on HL for the same longitudinal elements (μ = 0.51). However, contact pressure on the same VL surfaces is modeled using hard contact to describe the confinement of the geogrid in the *Y*–*Y* direction resulting from the soil interlocking within the geogrid aperture.

Transverse bars — The contact pressure developing on the transverse bars is described using the softened contact pressure–overclosure model. As explained earlier, when the pullout load is applied, frictional and bearing resistances will be mobilized along the interface between the soil and the geogrid. During pullout, the geogrid slides on the horizontal interfaces between the soil and the geogrid and frictional stresses are considered through the Coulomb friction model to resist slippage. In addition, under pullout loading, the geogrid penetrates the soil and as a result, contact pressures develop on the vertical surfaces of the transverse bars. As the test includes large deformation (around 25 mm applied displacement at the front side of the geogrid), the soft contact pressure–overclosure model is considered suitable and used here to simulate the contact pressure on the transverse bars. Using this model requires the definition of the contact stiffness (k_n) values, which relate the contact pressure on the transverse bar to the penetration distance into the soil. This parameter has to be calculated using the relative stiffness between the two contacting bodies. A large value of contact stiffness can reduce penetration; however, it can also cause convergence problems. Therefore, a proper contact stiffness value must be determined based on the allowable penetration, which requires some user experience. Most FE programs recommend that users start with a small initial k_n value that can be increased gradually until a reasonable penetration is achieved.

In this study, the propagation of the geogrid penetration into the soil is carefully investigated considering the experimental results. Understanding the geogrid penetration during pullout helps in selecting a proper k_n value that can be used to simulate the behavior of the transverse bars in the normal direction. The analysis involves 1012 contact surfaces. This number forms 506 contact pairs generated using the *automatic contact detection* tool available in ABAQUS and is optimized according to the required configurations.

Modeling the pullout process

After the FE model was built, the vertical stress (σ_v = 49 kPa) was applied simultaneously above and below the soil sample to maintain the geogrid in place before the test. Figure 8 shows the displacement field of the model after the application of the vertical pressure (σ_v = 49 kPa) at the top and bottom of the soil. It could be seen that the deformation values decreased from the upper and lower boundaries to reach 0 at the mid-height of the box where the geogrid layer is located. It should be highlighted that the vertical pressure is kept constant through the rest of the analysis.

Following the above step, the pullout load was introduced using a velocity control approach. Lateral velocity was applied to the rigid clamp in 10 steps (2.5 mm each), using the same rate used in the experiments (1 mm/min), to achieve a total frontal displacement (U_x) of 25 mm. Based on experience in analyzing similar problems, the velocity control scheme is found to improve the convergence of the analysis. It is worth noting that each pullout increment (step) was applied in 150 s with a velocity of 1.66×10^{-5} m/s (1 mm/min loading rate) to complete a total of 2.5 mm/step ($U_x = V_x \times \text{time} = 1.66 \times 10^{-5} \times 150 = 0.0025$ m or 2.5 mm/step, where V_x is the pullout velocity).

Results and discussions

Validation of numerical model

To validate the proposed model, the FE results are compared with the experimental data. Figure 9*a* shows the relationship between the pullout force and the frontal displacement obtained using both the experimental data and numerical analysis. The numerical results generally agreed with the experimental data except at low displacement levels of less than 5 mm. This may be attributed to the adopted simplification in modeling the thickness of the geogrid junction, which may result in underestimating the interaction between the soil and the geogrid, particularly at the early stages of the test.

To illustrate that the numerical model correctly calculates the geogrid response at the frontal face as well as at other locations along the geogrid, Fig. 9*b* shows a comparison between the calculated and measured displacements at different locations along the geogrid. Displacements generally decreased with distance from the face up to the middle of the geogrid. Very small displacements were calculated outside this region. The figure also confirms the agreement between the experimental and numerical results obtained using the proposed modeling approach.

By examining the displacement reduction along the geogrid (Fig. 9*b*), it can be seen that the rate of change in displacement is not constant. To shed some light on the role of k_n on the response of the system, a series of FE analyses was conducted where the stiffness coefficient (k_n) was incrementally varied with distance along the geogrid and the values that correspond to the observed response were determined. Figure 10 illustrates these k_n values that control the penetration at each transverse bar. Four contact stiffness values have been chosen at different locations. In contrast to the displacement distributions, the contact stiffness was found to increase with distance from the face (where the pullout load is applied) indicating a stiffer response of the soil–geogrid system inside the pullout box. It should be noted that k_n is kept constant beyond the middle of the geogrid length, which is consistent with the constant displacement found in this region.

Comparison with analytical solution

Several analytical methods are available to estimate the maximum pullout force (e.g., Peterson and Anderson 1980). Although these methods can reasonably estimate the maximum pullout force of a geosynthetic reinforcement, solutions specific to geogrid reinforcement are very limited. Figure 11 shows a summary of the measured and FE-calculated ultimate pullout resistances of the geogrid as compared to analytical solutions. It is found that the Peterson and Anderson (1980) solution, which assumes a general-failure mode for the passive bearing resistance, represents an upper value of the pullout resistance, whereas the analytical solution of Jewell et al. (1984), which assumes punching-

Fig. 8. Displacement field of soil and geogrid layer at (σ_v = 49 kPa). [Color online.]

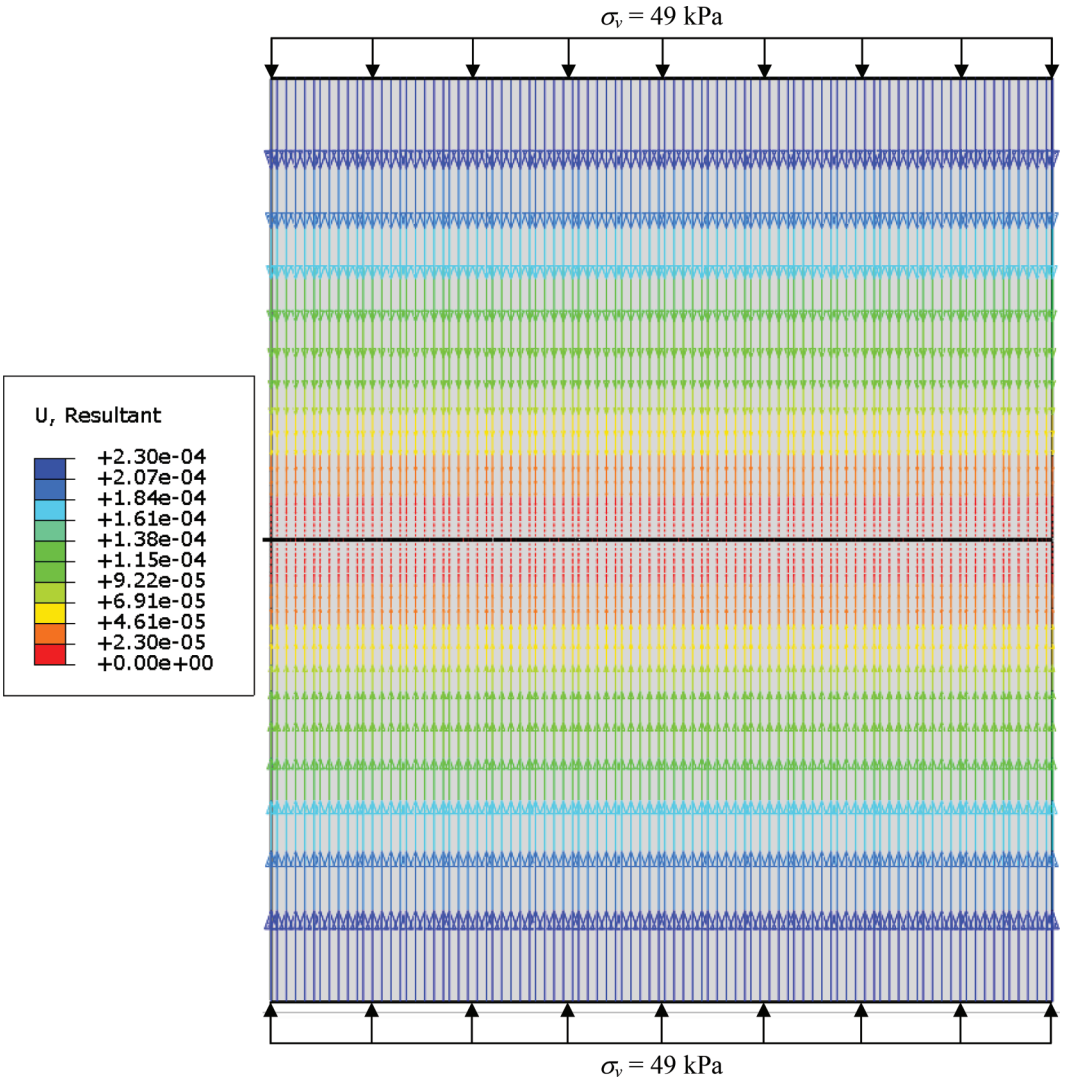

failure mode for the passive resistance, represents a lower bound for the pullout resistance. In addition, the results are compared with two other analytical procedures that have been developed for geotextile-reinforced soil (Weerasekara et al. 2017; Zornberg et al. 2017). The methods, however, assume constant shear resistance along the interface and ignore the bearing resistance of the transverse grid members. Therefore, the methods are expected to underestimate the pullout force as compared to the measured value or that calculated using 3D FE analysis.

Figure 11 also shows that both the experimental results and the FE predictions are located within the range of analytical solutions with tendency towards the upper bound line, particularly at low overburden pressures. This is attributed to the fact that at low confining pressure, dilatancy can have a significant effect on the soil–geogrid interaction. This behavior also signifies that the general failure mode of the passive resistance dominates the movement of the transverse geogrid members. Additional details related to the analytical studies of pullout resistance can be found elsewhere (Hussein 2016).

Response of geogrid

The deformed shape of the geogrid for a frontal displacement (U_x) of 10 mm and a vertical pressure (σ_v) of 49 kPa is shown in Fig. 12*a*. The largest geogrid deformation is found to occur near the applied load and decreases rapidly with distance towards the rear side of the box. The longitudinal elements of the geogrid experienced deformation in their axial direction with the largest elongation occurring near the loaded side. It should be noted that part of the geogrid that is connected directly to the loading clamp becomes unconfined immediately after the load application, which results in a softer behavior and larger elongation in that region. Transverse members, in contrast, showed considerable bending deformation, particularly near the loaded side. This bending behavior originates from the frictional forces acting at the upper and lower surfaces of the transverse bars as well as the bearing forces acting to resist the geogrid penetration into the soil. Figure 12*b* shows two additional patterns that describe the geogrid penetration into the soil located within the apertures ($Soil_{OPN}$). The transverse bars left their original locations and moved in the pullout loading direction. The distribution of the stresses developing in the geogrid is shown in Fig. 13. Consistent with the displacement pattern, the stresses S_{xx} were maximum near the front side and decreased with distance along the geogrid. It can be also realized that stresses in the longitudinal members are much larger compared to the transverse bars.

The tensile force distributions in the longitudinal members for different frontal displacements are illustrated in Fig. 14. At a given location along the geogrid, the average tensile force (T_{xx}) in all longitudinal members was found to increase with the increase in

Fig. 9. Pullout response of geogrid (σ_v = 49 kPa). [Color online.]

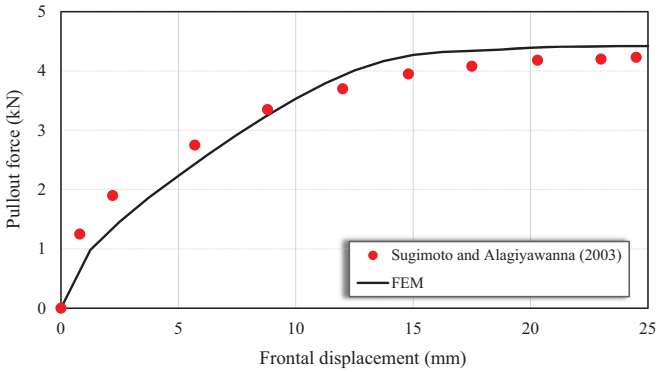

a) Pullout load-frontal displacement relationship

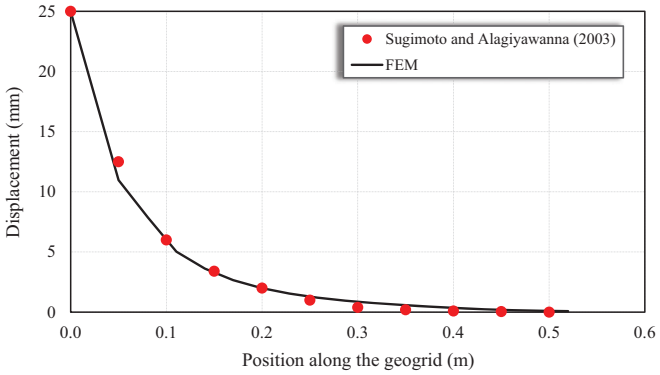

b) Horizontal displacement along the geogrid

Fig. 10. Suggested changes of k_n values on transverse bars along geogrid. [Color online.]

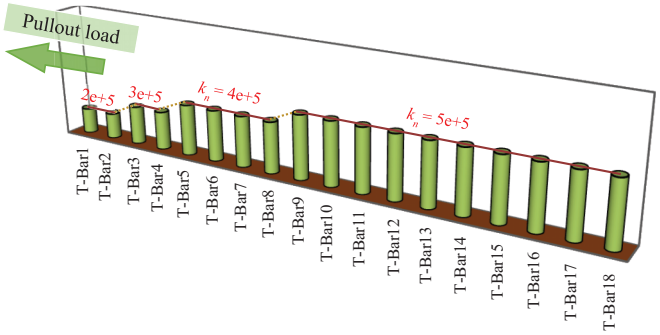

frontal displacements. For the considered range of frontal displacements, the force T_{xx} was large near the front side and decreased rapidly towards the middle of the geogrid. Beyond the middle area, T_{xx} became negligibly small due to the insignificant displacement experienced by the rest of the geogrid.

Contributions of bearing and frictional resistances

The geogrid used comprises longitudinal and transverse members as well as junctions connecting these members. Each of these components contributes to the total pullout force. As the resistance of the junctions is considered in the frictional resistance of the geogrid, the total pullout resistance (F_{pull}) can be written as

$$F_{pull} = F_{friction} + F_{bearing} \quad (4)$$

where $F_{friction}$ is the frictional resistance component arising from the geogrid surface and $F_{bearing}$ is the bearing resistance of the transverse members.

To understand the separate contributions of the bearing and frictional resistances, researchers usually test the geogrid in the laboratory with and without transverse bars by removing the bars that are responsible for developing the bearing resistance (e.g., Alagiyawanna et al. 2001). Similarly, researchers have followed this elimination procedure in numerical analysis (e.g., Wang et al. 2016). This technique is not recommended by the authors as removing the transverse bars will result in both frictional and passive bearing resistances being eliminated.

To assess the contribution of the bearing component in the present study, the transverse bars are kept with their frictional resistance in the original geometry; however, the k_n (contact stiffness) parameter that controls the bearing resistance is reduced. By reducing the k_n value in the normal direction (on the surfaces of the transverse bars VT) to 0, the bearing resistance developing on these members will diminish. This technique will eliminate the bearing resistance only from the transverse bars; however, the effect of the frictional resistance on the horizontal surfaces of the transverse bars (HT) remains the same. As a k_n value of 0 can cause numerical instability, a value of k_n = 0.0001 was selected for the analysis.

To understand the cumulative contributions of the 18 transverse bars towards the total pullout resistance, a procedure that includes six different steps was developed and implemented employing six separate analyses. In each step, the bearing resistance component is de-activated (i.e., k_n is set to 0.0001) for a group of three transverse bars along the geogrid. This procedure is illustrated in Fig. 15.

The bearing resistances on the transverse bars are determined numerically using the previous procedure and the cumulative contribution to the total pullout force is presented in Fig. 16. It is evident that decreasing the number of transverse members in six equal steps (from 18 members in step-1 to zero members in step-6) decreases the total pullout load and increases the relative movement of the geogrid.

Comparing the results of the original configuration with the results of step-6 where no bearing members contribute to the total pullout force allows one to calculate the frictional resistance component. The separate contributions to the total pullout resistance is shown in Fig. 17. It can be seen that the contribution of the frictional resistance is less than that of the bearing resistance leading to the bearing component ($F_{bearing}$) dominating the pullout resistance (F_{pull}). The frictional component contributed about 28% of the total pullout load. Similar observations were made by previous researchers (e.g., Milligan and Palmeira 1987; Bergado and Chai 1994; Lopes and Lopes 1999) confirming that, in this class of problems, the bearing resistance component is generally larger than the frictional component.

Another way to understand soil–geogrid interaction mechanism is by comparing the pullout response with that of an equivalent planer sheet with no openings. Modeling a geogrid using a planer sheet generally requires extensive calibration to balance the increase in geometric stiffness associated with the continuous nature of the sheet. This has been usually used by researchers to simplify 3D models involving geogrid-reinforced soils (Huang et al. 2005). In these cases, only frictional resistance is mobilized in the reinforcement layer, which may not reflect the actual geogrid response. To illustrate the level of inaccuracy associated with such simplification, a numerical model was developed using a planer sheet (52 cm × 30 cm). The biaxial geogrid, used in this study, involves an open area of about 70%. This corresponds to an equivalent sheet thickness of 0.175 mm as recommended by Hussein and Meguid (2016). The pullout response of the geogrid is compared with the equivalent planer sheet as shown in Fig. 18. Modeling the biaxial geogrid as a planer sheet resulted in a reduction in the total pullout resistance of about 30%. This confirms the previous finding that the bearing component contributes significantly to the overall resistance. In addition, it is found that the planer sheet initially exhibits a stiffer response at a low

Fig. 11. Comparison between analytical and numerical results of pullout resistance. [Color online.]

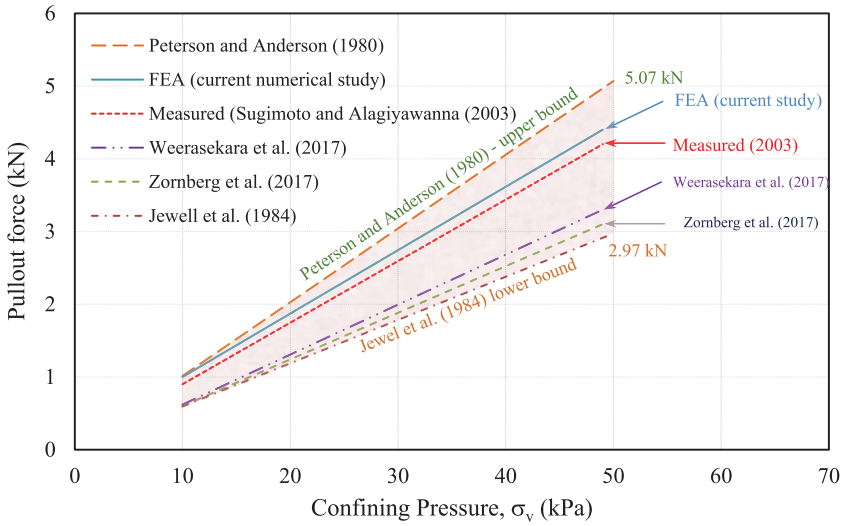

Fig. 12. Geogrid deformation and relative movements. [Color online.]

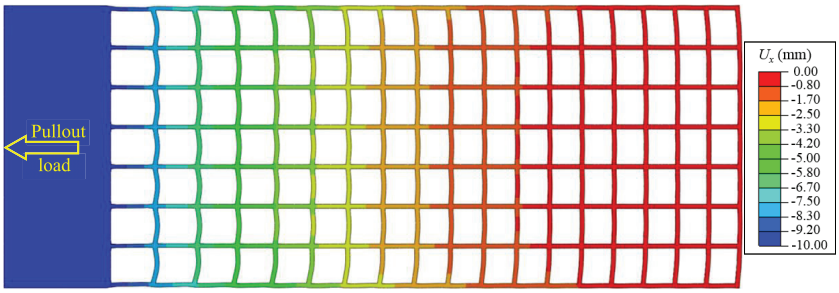

a) Geogrid deformed shape and displacement at $U_x = 10$ mm and $\sigma_v = 49$ kPa

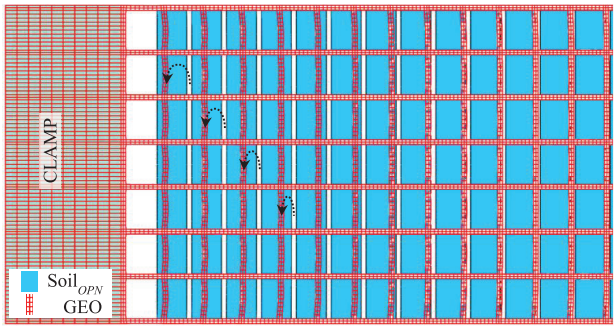

Geogrid versus $Soil_{OPN}$

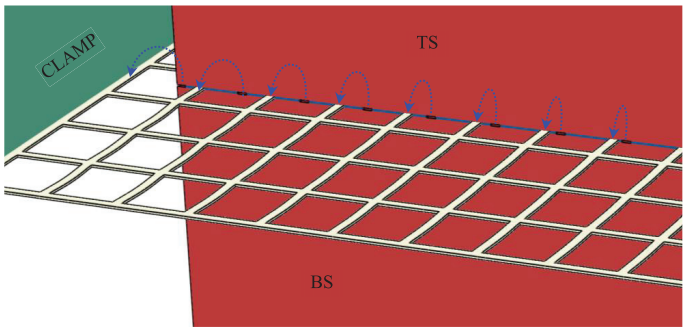

Geogrid versus TS and BS

b) Relative movements between geogrid and the backfill soil

Fig. 13. Geogrid stresses S_{xx} at U_x = 10 mm and σ_v = 49 kPa. [Color online.]

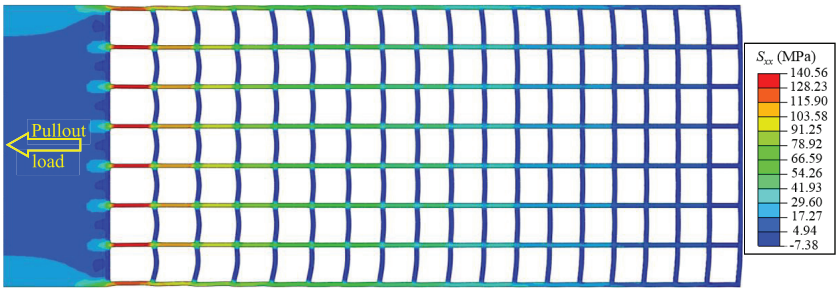

Fig. 14. Average tensile force T_{xx} in longitudinal members (σ_v = 49 kPa). [Color online.]

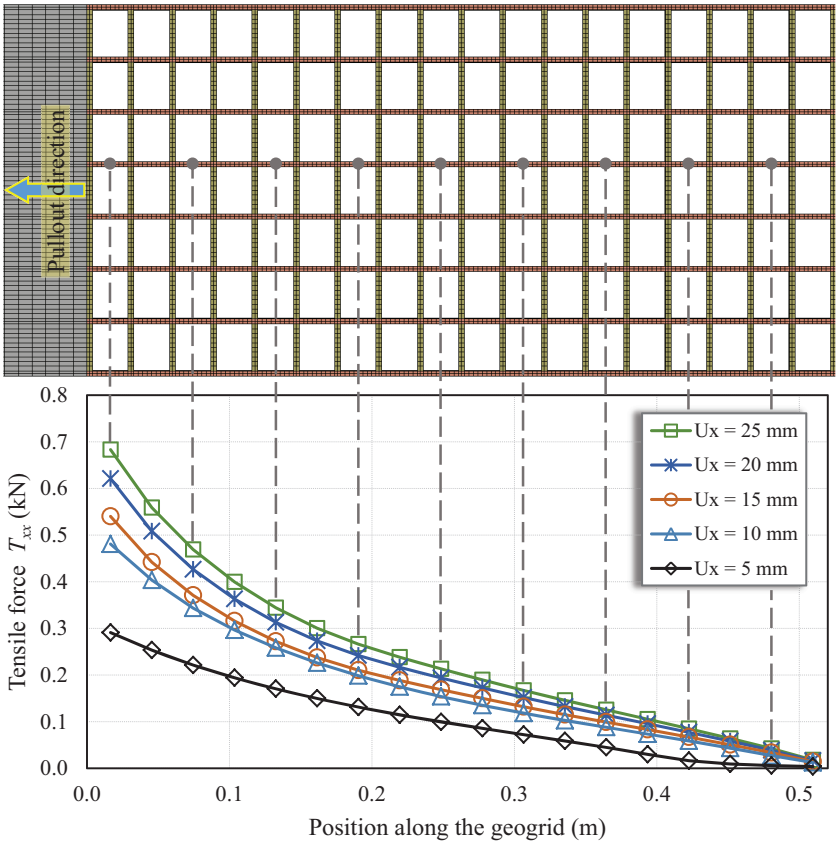

Fig. 15. Procedure to assess accumulative contributions of bearing members. [Color online.]

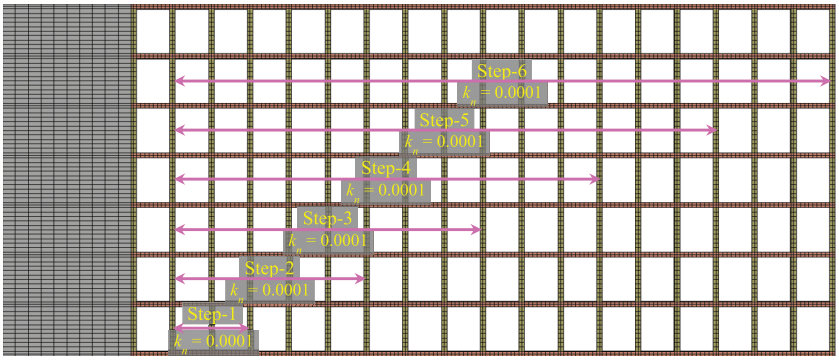

deformation range. This is attributed to the limited elongation experienced by the continuous sheet as compared with that experienced by the longitudinal ribs before the bearing resistance of the transverse ribs is activated.

Figure 19 shows the relationship between the bearing resistance and the frontal displacement up to U_x = 10 mm. Contact pressure on the transverse bars is found to increase with the increase of applied displacement, with maximum pressure calcu-

Fig. 16. Cumulative contribution of bearing members to total pullout resistance: (*a*) pullout force; (*b*) geogrid displacement. [Color online.]

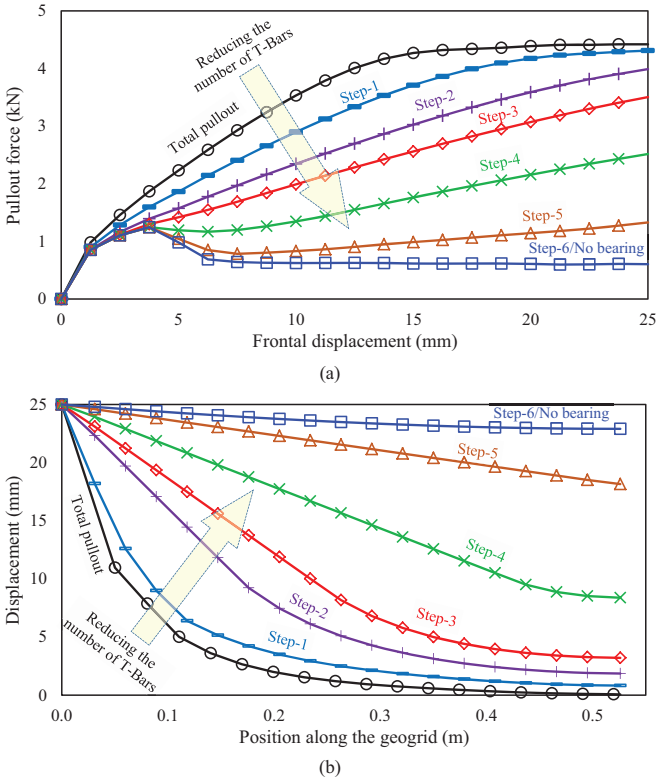

Fig. 17. Components of pullout resistance (σ_v = 49 kPa). [Color online.]

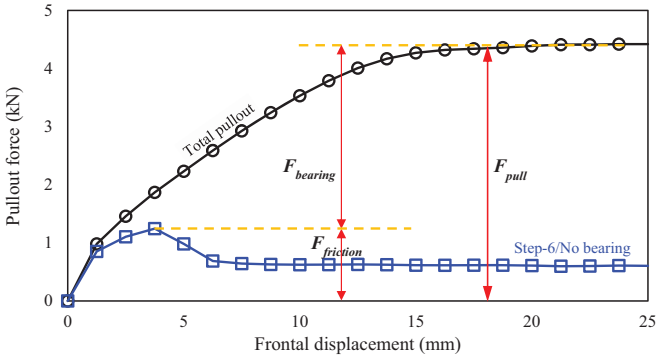

lated near the location of the applied load, which decreases gradually with distance from the load. It should be noted that only selected bars are presented in this figure, however, the same trend applies to all the transverse members.

The accumulated contribution of different transverse members ($T_{bearing/member}$) with respect to the total bearing resistance ($T_{bearing}$) is shown in Fig. 20. In the original configuration (Fig. 20*a*), the cumulative contribution of the members located within the first half of the geogrid (Nos. 1 through 9) measured from the front side was found to be about 90% of the total bearing resistance. In general, the first transverse member (counted from the loaded end) contributed the most to the overall bearing resistance and the contributions of transverse members decreased with distance from the loaded side. When bearing members are progressively eliminated (Figs. 20*b*, 20*c*, and 20*d*), the remaining transverse members start resisting the penetration of the first effective transverse bar, which has been found to carry around 20% of the total bearing resistance.

Fig. 18. Comparison of pullout force for actual geogrid and planer sheet. [Color online.]

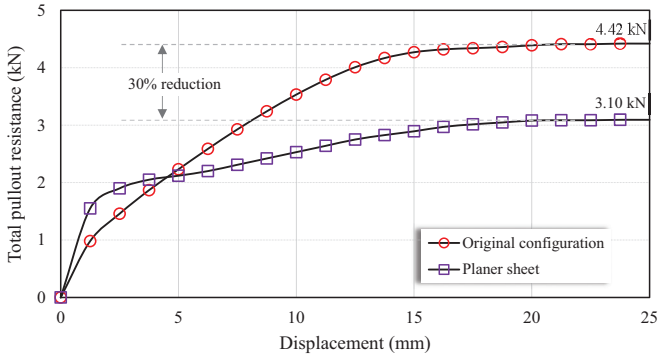

Fig. 19. Contact pressure developed on T-bars versus frontal displacement. [Color online.]

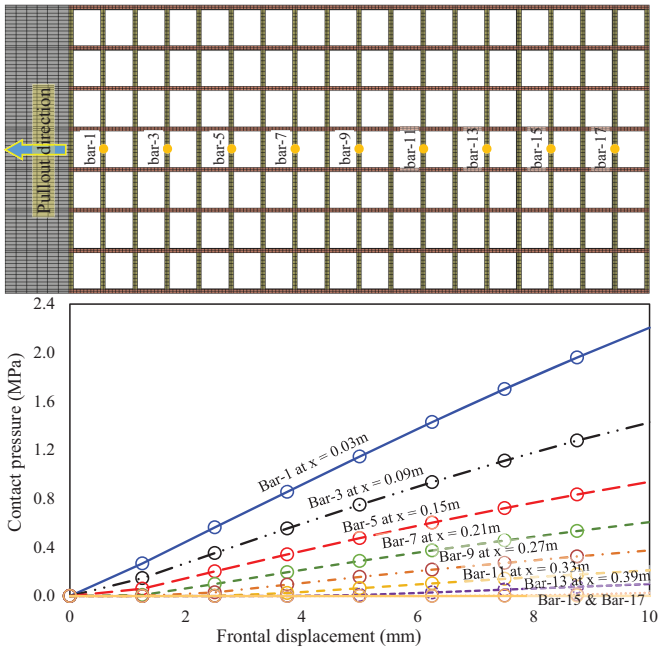

A normalized comparison between the initial geogrid geometry (with 18 transverse bars) and the investigated cases with selected active members is depicted in Fig. 21. De-activating half of the transverse members (step-3) resulted in a reduction of the bearing resistance by about 50% and hence only half of the pullout capacity becomes available in the system.

The change in tensile forces in the geogrid under different configurations, with references to Fig. 15, is further examined by plotting the changes in tensile forces for the investigated scenarios as illustrated in Fig. 22. It can be seen that, for the original configuration, the tensile forces in the longitudinal ribs decrease with distance along the geogrid. De-activating transverse bars causes the tensile forces to become constant for the distance where no transverse bars existed and then starts to decrease with distance towards the free end. This is attributed to the absence of confinement in the areas where transverse bars are absent. For example, in step-4, the tensile force was constant at a value of 0.2 kN up to a distance of 0.34 m then decreased to 0 at the free end. This constant load is similar to that of the tensile stresses that develop when a geogrid is tested in air where no confinement existed and the role of the transverse ribs in carrying tensile load is very minimum (Hussein and Meguid 2016).

Fig. 20. Contribution of transverse members to total bearing resistance (U_x = 10 mm). [Color online.]

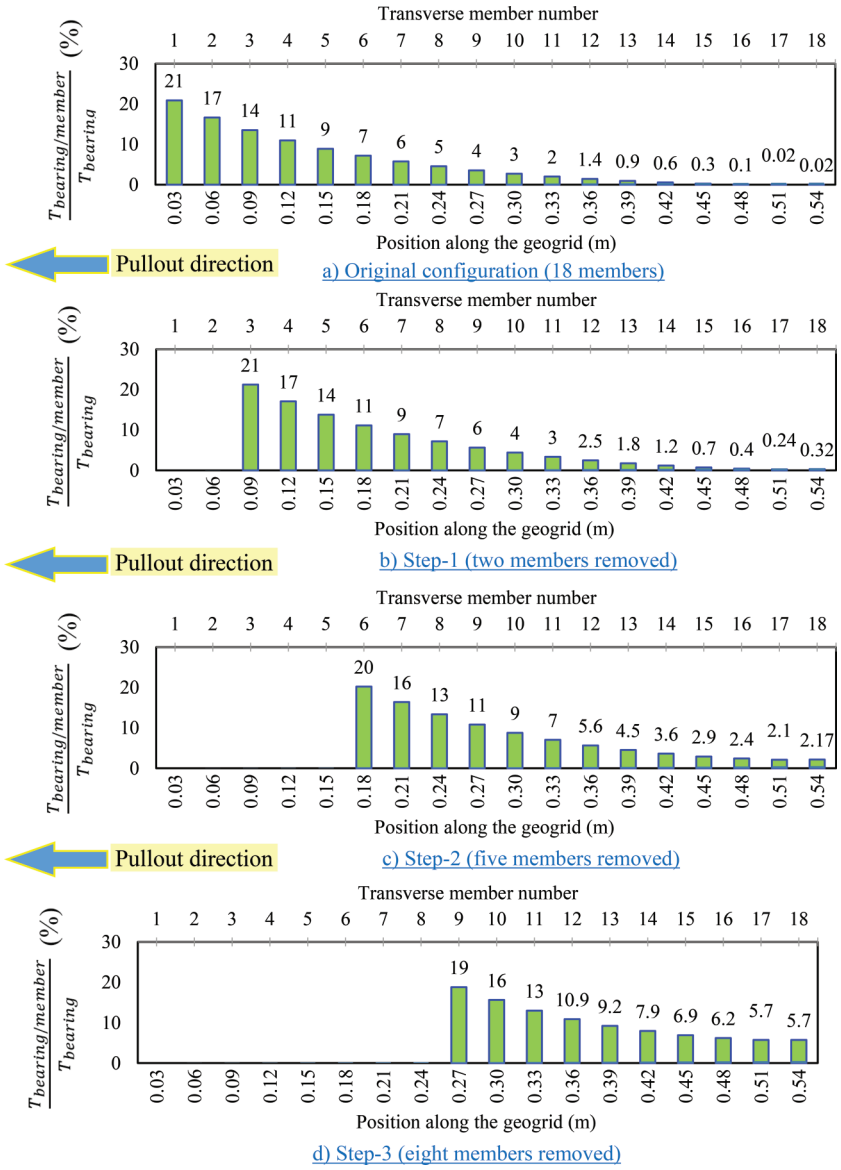

Fig. 21. Effect of removing transverse bars. [Color online.]

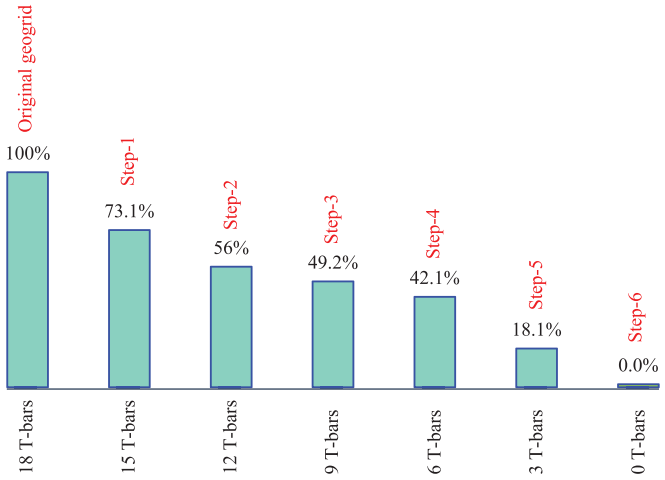

Response of backfill material

The vertical stress distribution is calculated on a horizontal plane located 50 mm above the geogrid and the results are presented in Fig. 23. This location was chosen to avoid stress concentration zones located at the geogrid location. Before the pullout starts (U_x = 0 mm; initial condition), the vertical stress distribution is approximately constant and equal to the applied vertical stress (σ_v = 49 kPa). With the increase in frontal displacement, an increase in the vertical stress is calculated with a maximum value developing at the front face. Similar observations were made by Tran et al. (2013) and Wang et al. (2016). This increase in pressure is attributed to the fact that geogrid movement towards the front wall generates additional horizontal forces, which restrain the soil dilatancy near the boundary.

Figure 24 shows the displacement field in the soil domain at a frontal displacement of 10 mm. It can be seen that most of the soil movement is concentrated near the front face of the box, leading to soil densification in that area. Away from the pullout zone, soil movement was mostly vertical pointing towards the geogrid. This displacement pattern changed at the geogrid location where movements became more horizontal pointing to the pullout di-

Fig. 22. Change in tensile forces under different conditions at U_x = 10 mm. [Color online.]

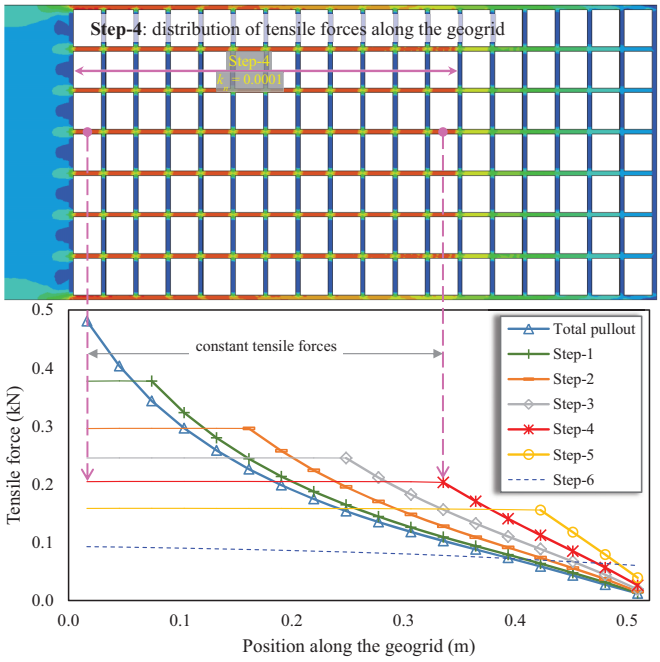

Fig. 23. Distribution of vertical stresses (S_{zz}) in backfill material. [Color online.]

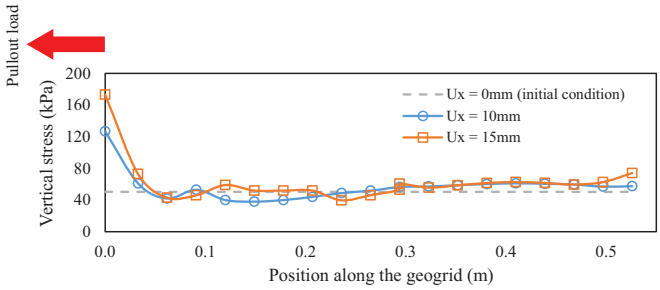

rection. At the front wall, vertical movement was found where soil particles started to move away from the geogrid. These observations agree well with the results of the X-ray radiographs reported by Sugimoto et al. (2001). Similar soil movement pattern in pullout tests has also been reported by Jewell (1980) and Dyer (1985).

Figure 25 illustrates the AC YIELD (actively yielding) zone, which is a scalar quantity denoting the onset of soil yielding. A value of 0 indicates that the soil has not yielded, and a value of 1.0 indicates that the soil has yielded and plastic strains have developed during that loading increment. The shape of the plastic strain in this figure represents the plasticity developing immediately in front of the bearing members, which is consistent with the theoretical bearing resistance mechanism described by Jewell et al. (1984) and Dyer (1985). The size of the developed plasticity zone was found to increase with the increase in applied frontal displacement.

Summary and conclusions

This study investigated the pullout behavior of a biaxial geogrid embedded in granular soil using 3D FE analysis. In developing the FE model, the details of the geometrical features of the geogridwere explicitly simulated. The geogrid was modeled using an elastoplastic constitutive model that has been previously developed and validated by the authors. The backfill material was simulated

Fig. 24. Displacement field of soil specimen at U_x = 10 mm. [Color online.]

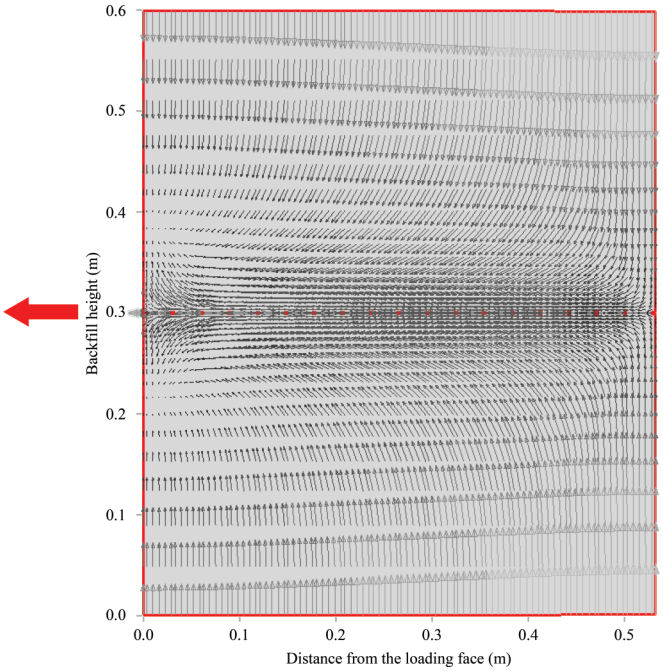

Fig. 25. Contour plot of AC YIELD in backfill soil at U_x = 10 mm. [Color online.]

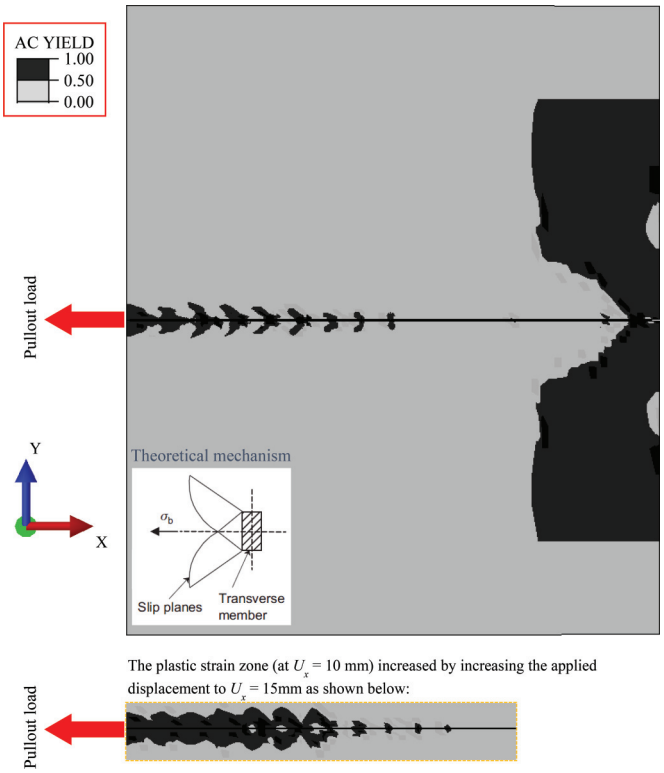

using the Mohr–Coulomb failure criterion. A detailed procedure of the contact modeling technique used in the analysis was described. This includes the contact constitutive models in both the tangential and normal directions, the contact discretization, and the constraints evolution. A softened contact pressure–overclosure model was used to simulate the behavior of the transverse mem-

bers. This model is governed by a penalty stiffness parameter that has been calibrated in this study using the actual displacement distributions obtained from the experimental data. The displacements and stresses developing in the geogrid were calculated and the backfill movements and plastic strains developing in the soil were investigated.

Most of the geogrid stresses and displacements occurred near the front side of the box with rapid decrease with distance towards the middle of the geogrid. The load-transfer mechanism was investigated by examining the distribution of the tensile forces, contact pressures, and the displacements along the geogrid while progressively de-activating selected transverse members. This was achieved in six separate steps and the contributions of the frictional and bearing resistance components to the total pullout load was evaluated. For the investigated geogrid and soil conditions, the contribution of the bearing resistance to the total pullout capacity was found to be larger than the frictional resistance. The contribution of the bearing resistance was found to increase as the geogrid displacement increased and the total capacity decreased with reduction in the number of bearing members. The accumulated contribution of the different transverse members to the total bearing resistance was also evaluated. The first transverse member contributed the largest to the total bearing resistance and the contributions of the transverse members decreased with distance from the loaded side.

Soil movement and stresses agreed reasonably well with experimental observations. An increase in soil stresses was found near the front face. The calculated plastic strain patterns were found to be consistent with the theoretical approaches. Finally, the proposed FE approach has been proven efficient in modeling the pullout experiment in three-dimensions and capturing the response of both the geogrid and the surrounding backfill material.

Acknowledgement

This research is supported by the Natural Sciences and Engineering Research Council of Canada (NSERC) grant No. RGPIN-2016-05263.

References

AASHTO. 2012. LRFD bridge design specifications. 6th ed. American Association of State Highway and Transportation Officials, Washington, D.C., USA.

Abdi, M.R., and Mirzaeifar, H. 2017. Experimental and PIV evaluation of grain size and distribution on soil–geogrid interactions in pullout test. Soils and Foundations, **57**(6): 1045–1058. doi:10.1016/j.sandf.2017.08.030.

Abdi, M.R., and Zandieh, A.R. 2014. Experimental and numerical analysis of large scale pull out tests conducted on clays reinforced with geogrids encapsulated with coarse material. Geotextiles and Geomembranes, **42**(5): 494–504. doi:10.1016/j.geotexmem.2014.07.008.

Alagiyawanna, A.M.N., Sugimoto, M., Sato, S., and Toyota, H. 2001. Influence of longitudinal and transverse members on geogrid pullout behavior during deformation. Geotextiles and Geomembranes, **19**(8): 483–507. doi:10.1016/S0266-1144(01)00020-6.

ASTM. 2013. Standard test method for measuring geosynthetic pullout resistance in soil. ASTM standard D6706-01. ASTM International. West Conshohocken, PA, USA.

Bakeer, R.M., Sayed, S.M., Cates, P., and Subramanian, R. 1998. Pullout and shear tests on geogrid reinforced lightweight aggregate. Geotextiles and Geomembranes, **16**(2): 119–133. doi:10.1016/S0266-1144(97)10025-5.

Bathurst, R.J., and Ezzein, F.M. 2016. Geogrid pullout load-strain behaviour and modelling using a transparent granular soil. Geosynthetics International, **23**(4): 271–286. doi:10.1680/jgein.15.00051.

Berg, R.R., Christopher, B.R., and Samtani, N.C. 2009. Design of mechanically stabilized earth walls and reinforced soil slopes - Volume I. U.S. Department of Transportation - FHWA, Report No. FHWA-NHI-10-024. NHI - National Highway Institute, Woodbury, Minnesota, USA.

Bergado, D.T., and Chai, J.-C. 1994. Pullout force/displacement relationship of extensible grid reinforcements. Geotextiles and Geomembranes, **13**(5): 295–316. doi:10.1016/0266-1144(94)90025-6.

Bhandari, A., and Han, J. 2010. Investigation of geotextile-soil interaction under a cyclic vertical load using the discrete element method. Geotextiles and Geomembranes, **28**(1): 33–43. doi:10.1016/j.geotexmem.2009.09.005.

Bolton, M.D. 1986. The strength and dilatancy of sands. Géotechnique, **36**(1): 65–78. doi:10.1680/geot.1986.36.1.65.

Cardile, G., Moraci, N., and Calvarano, L.S. 2016. Geogrid pullout behaviour according to the experimental evaluation of the active length. Geosynthetics International, **23**(3): 194–205. doi:10.1680/jgein.15.00042.

Cardile, G., Gioffrè, D., Moraci, N., and Calvarano, L.S. 2017. Modelling interference between the geogrid bearing members under pullout loading conditions. Geotextiles and Geomembranes, **45**(3): 169–177. doi:10.1016/j.geotexmem.2017.01.008.

Chen, C., McDowell, G.R., and Thom, N.H. 2012. Discrete element modelling of cyclic loads of geogrid-reinforced ballast under confined and unconfined conditions. Geotextiles and Geomembranes, **35**: 76–86. doi:10.1016/j.geotexmem.2012.07.004.

Chen, R., Luan, M., and Hao, D. 2011. Improved simulation method for soil-geogrid interaction of reinforced earth structure in FEM. Transactions of Tianjin University, **17**(3): 220–228. doi:10.1007/s12209-011-1528-1.

Dassault Systems Simulia Corp. 2013. ABAQUS user's manuals. Version 6.13. Dassault Systems Simulia Corp., Providence, USA.

Dyer, M.R. 1985. Observation of the stress distribution in crushed glass with applications to soil reinforcement. Ph.D. thesis, Department of Engineering Science, University of Oxford, Oxford, UK.

Farrag, K., Acar, Y.B., and Juran, I. 1993. Pull-out resistance of geogrid reinforcements. Geotextiles and Geomembranes, **12**(2): 133–159. doi:10.1016/0266-1144(93)90003-7.

Ferreira, F.B., Vieira, C.S., Lopes, M.L., and Carlos, D.M. 2015. Experimental investigation on the pullout behaviour of geosynthetics embedded in a granite residual soil. European Journal of Environmental and Civil Engineering, **20**(9): 1147–1180. doi:10.1080/19648189.2015.1090927.

Gu, J., Zhang, M., and Dai, Z. 2018. Numerical and experimental investigation of tensile behavior of geogrids with circular and square apertures. *In* Proceedings of GeoShanghai 2018: International Conference in Ground Improvement and Geosynthetics. Springer, Singapore.

Gurung, N., and Iwao, Y. 1999. comparative model study of geosynthetic pull-out response. Geosynthetics International, **6**(1): 53–68. doi:10.1680/gein.6.0143.

Hatami, K., Mahmood, T., Ghabchi, R., and Zaman, M. 2013. Influence of in-isolation properties of geogrids on their pullout performance in a dense graded aggregate. Indian Geotechnical Journal, **43**(4): 303–320. doi:10.1007/s40098-013-0060-8.

Hegde, A., and Roy, R. 2017. A comparative numerical study on soil–geosynthetic interactions using large scale direct shear test and pullout test. International Journal of Geosynthetics and Ground Engineering, **4**(1): 2. doi:10.1007/s40891-017-0119-1.

Huang, J., Han, J., and Collin, J.G. 2005. Geogrid-reinforced pile-supported railway embankments: a three-dimensional numerical analysis. Transportation Research Record, **1936**: 221–229. doi:10.1177/0361198105193600125.

Hussein, M.G. 2016. Numerical modeling framework for soil-geosynthetics interaction problems. Ph.D. thesis, Department of Civil Engineering and Applied Mechanics, McGill University, Montréal, Canada.

Hussein, M.G., and Meguid, M.A. 2009. On the 3D modelling of soil-geogrid interaction. *In* Proceedings of GeoHalifax 2009, the 62nd Canadian Geotechnical Conference, Halifax, Canada. Canadian Geotechnical Society. Paper No. 138, pp. 986–991.

Hussein, M.G., and Meguid, M.A. 2013. Three-dimensional finite element analysis of soil-geogrid interaction under pull-out loading condition. *In* Proceedings of GeoMontreal 2013, the 66th Canadian Geotechnical Conference, Montreal, Canada. Canadian Geotechnical Society. Paper No. 260, pp. 452–458.

Hussein, M.G., and Meguid, M.A. 2016. A three-dimensional finite element approach for modeling biaxial geogrid with application to geogrid-reinforced soils. Geotextiles and Geomembranes, **44**(3): 295–307. doi:10.1016/j.geotexmem.2015.12.004.

Jewell, R.A. 1980. Some effects of reinforcement on the mechanical behaviour of soils. Ph.D. thesis, Department of Engineering: Civil Engineering Devision, University of Cambridge, Cambridge, UK.

Jewell, R.A., Milligan, G.W.E., Sarsby, R.W., and Dubois, D. 1984. Interaction between soil and geogrid. *In* Proceedings of Polymer Grid Reinforcement. Thomas Telford, London, UK. pp. 18–30.

Kayadelen, C., Önal, T.Ö., and Altay, G. 2018. Experimental study on pull-out response of geogrid embedded in sand. Measurement, **117**: 390–396. doi:10.1016/j.measurement.2017.12.024.

Koerner, R.M. 2012. Designing with Geosynthetics. 6th ed. Xlibris Corporation, USA. Vols. 1 and 2.

Koerner, R.M., Wayne, M.H., and Carroll, R.G. 1989. Analytic behavior of geogrid anchorage. *In* Proceedings of Geosynthetics '89, IFAI San Diego, San Diego, California, USA. pp. 525–536.

Lentz, R.W., and Pyatt, J.N. 1988. Pull-out resistance of geogrids in sand. Transportation Research Record, **1188**: 48–55.

Liu, C., Zornberg, J., Chen, T., Ho, Y., and Lin, B. 2009. Behavior of geogrid-sand interface in direct shear mode. Geotechnical and Geoenvironmental Engineering, **135**(12): 1863–1871. doi:10.1061/(ASCE)GT.1943-5606.0000150.

Lopes, M.J., and Lopes, M.L. 1999. Soil-geosynthetic interaction-influence of soil particle size and geosynthetic structure. Geosynthetics International, **6**(4): 261–282. doi:10.1680/gein.6.0153.

Lopes, M.L., and Silvano, R. 2010. Soil/geotextile interface behaviour in direct shear and pullout movements. Geotechnical and Geological Engineering, **28**(6): 791–804. doi:10.1007/s10706-010-9339-z.

Lopes, P.C., Lopes, M.L., and Lopes, M.P. 2001. Shear behaviour of geosynthetics in the inclined plane test – influence of soil particle size and geosynthetic structure. Geosynthetics International, **8**(4): 327–342. doi:10.1680/gein.8.0198.

McDowell, G.R., Harireche, O., Konietzky, H., Brown, S.F., and Thom, N.H. 2006. Discrete element modelling of geogrid-reinforced aggregates. Proceedings of the Institution of Civil Engineers - Geotechnical Engineering, **159**(1): 35–48. doi:10.1680/geng.2006.159.1.35.

McGown, A., Andrawes, K.Z., Yeo, K.C., and DuBois, D. 1984. The load-strain-time behaviour of tensar geogrids. *In* Proceedings of Polymer Grid Reinforcement. Thomas Telford, London, UK. pp. 11–17.

Meguid, M.A. 2014. Recent developments in numerical modelling of composite systems with geogrid inclusions. *In* Proceedings of the International Workshop on Advanced Composites for Engineering Applications (ACEA 2014), The German University in Cairo, Cairo, Egypt. pp. 13–26.

Miao, C., Zheng, J., Zhang, R., and Cui, L. 2017. DEM modeling of pullout behavior of geogrid reinforced ballast: the effect of particle shape. Computers and Geotechnics, **81**: 249–261. doi:10.1016/j.compgeo.2016.08.028.

Milligan, G.W.E., and Palmeira, E.P. 1987. Prediction of bond between soil and reinforcement. *In* Proceedings of the International Symposium on Prediction and Performance in Geotechnical Engineering, Calgary, Canada. pp. 147–153.

Moraci, N., and Gioffrè, D. 2006. A simple method to evaluate the pullout resistance of extruded geogrids embedded in a compacted granular soil. Geotextiles and Geomembranes, **24**(2): 116–128. doi:10.1016/j.geotexmem.2005.11.001.

Moraci, N., and Recalcati, P. 2006. Factors affecting the pullout behaviour of extruded geogrids embedded in a compacted granular soil. Geotextiles and Geomembranes, **24**(4): 220–242. doi:10.1016/j.geotexmem.2006.03.001.

Moraci, N., Cardile, G., Gioffrè, D., Mandaglio, M.C., Calvarano, L.S., and Carbone, L. 2014. Soil geosynthetic interaction: design parameters from experimental and theoretical analysis. Transportation Infrastructure Geotechnology, **1**(2): 165–227. doi:10.1007/s40515-014-0007-2.

Palmeira, E.M., and Milligan, G.W.E. 1989. Scale and other factors affecting the results of pull-out tests of grids buried in sand. Géotechnique, **39**(3): 511–542. doi:10.1680/geot.1989.39.3.511.

Perkins, S.W., and Cuelho, E.V. 1999. Soil-geosynthetic interface strength and stiffness relationships from pullout tests. Geosynthetics International, **6**(5): 321–346. doi:10.1680/gein.6.0156.

Perkins, S.W., and Edens, M.Q. 2003. Finite element modeling of a geosynthetic pullout test. Geotechnical and Geological Engineering, **21**(4): 357–375. doi:10.1023/B:GEGE.0000006053.77489.c5.

Peterson, L.M., and Anderson, L.R. 1980. Pullout resistance of welded wire mesh embedded in soil. Research Report Submitted to Hilfiker Pipe Co. Department of Civil Engineering at Utah State University, Logan, Utah, USA.

Shuwang, Y., Shouzhong, F., and Barr, B. 1998. Finite-element modelling of soil-geogrid interaction dealing with the pullout behaviour of geogrids. Acta Mechanica Sinica, **14**(4): 371–382. doi:10.1007/BF02486875.

Siriwardane, H., Gondle, R., Kutuk, B., and Ingram, R. 2008. Experimental investigation and numerical analysis of reinforced geologic media. *In* Proceedings of the 12th International Conference of International Association for Computer Methods and Advances in Geomechanics (IACMAG), Goa, India. pp. 4369–4376.

Sugimoto, M., and Alagiyawanna, A.M.N. 2003. Pullout behavior of geogrid by test and numerical analysis. Journal of Geotechnical and Geoenvironmental Engineering, **129**(4): 361–371. doi:10.1061/(ASCE)1090-0241(2003)129:4(361).

Sugimoto, M., Alagiyawanna, A.M.N., and Kadoguchi, K. 2001. Influence of rigid and flexible face on geogrid pullout tests. Geotextiles and Geomembranes, **19**(5): 257–277. doi:10.1016/S0266-1144(01)00011-5.

Touahmia, M., Rouili, A., Boukendakdji, M., and Achour, B. 2018. Experimental and numerical analysis of geogrid-reinforced soil systems. Arabian Journal for Science and Engineering, **34**(10): 5295–5303.

Tran, V.D.H., Meguid, M.A., and Chouinard, L.E. 2013. A finite-discrete element framework for the 3D modeling of geogrid-soil interaction under pullout loading conditions. Geotextiles and Geomembranes, **37**: 1–9. doi:10.1016/j.geotexmem.2013.01.003.

Wang, Z., Jacobs, F., and Ziegler, M. 2016. Experimental and DEM investigation of geogrid-soil interaction under pullout loads. Geotextiles and Geomembranes, **44**(3): 230–246. doi:10.1016/j.geotexmem.2015.11.001.

Weerasekara, L., Hall, B., and Wijewickreme, D. 2017. A new approach for estimating internal stability of reinforced soil structures. Geosynthetics International, **24**(4): 419–434. doi:10.1680/jgein.17.00012.

Wilson-Fahmy, R.F., and Koerner, R.M. 1993. Finite element modelling of soil-geogrid interaction with application to the behavior of geogrids in a pullout loading condition. Geotextiles and Geomembranes, **12**(5): 479–501. doi:10.1016/0266-1144(93)90023-H.

Xu, C., and Liang, C. 2018. DEM Simulation of pullout tests of geogrid-reinforced gravelly sand. *In* Proceedings of GeoShanghai 2018: International Conference in Ground Improvement and Geosynthetics. Springer, Singapore.

Yuan, Z., and Chua, K.M. 1990. Numerical evaluation of the pullout box method for studying soil-reinforcement interaction. Transportation Research Record, **1278**: 116–124.

Zhang, J., Yasufuku, N., and Ochiai, H. 2008. discrete element modelling of geogrid pullout test. *In* Proceedings of the 4th Asian Regional Conference on Geosynthetics. Shanghai, China. pp. 11–14.

Zornberg, J.G., Roodi, G.H., and Gupta, R. 2017. Stiffness of soil-geosynthetic composite under small displacements: I. model development. Journal of Geotechnical and Geoenvironmental Engineering, **143**(10): 1–13. doi:10.1061/(ASCE)GT.1943-5606.0001768.